A TNF–JNK–Axl–ERK signaling axis mediates primary resistance to EGFR inhibition in glioblastoma

Gao Guo[1], Ke Gong[1], Sonia Ali[1], Neha Ali[1], Shahzad Shallwani[1], Kimmo J Hatanpaa[2], Edward Pan[1], Bruce Mickey[3], Sandeep Burma[4], David H Wang[5,6], Santosh Kesari[7], Jann N Sarkaria[8], Dawen Zhao[9] & Amyn A Habib[1,6]

Aberrant epidermal growth factor receptor (EGFR) signaling is widespread in cancer, making the EGFR an important target for therapy. *EGFR* gene amplification and mutation are common in glioblastoma (GBM), but EGFR inhibition has not been effective in treating this tumor. Here we propose that primary resistance to EGFR inhibition in glioma cells results from a rapid compensatory response to EGFR inhibition that mediates cell survival. We show that in glioma cells expressing either EGFR wild type or the mutant EGFRvIII, EGFR inhibition triggers a rapid adaptive response driven by increased tumor necrosis factor (TNF) secretion, which leads to activation in turn of c-Jun N-terminal kinase (JNK), the Axl receptor tyrosine kinase and extracellular signal–regulated kinases (ERK). Inhibition of this adaptive axis at multiple nodes rendered glioma cells with primary resistance sensitive to EGFR inhibition. Our findings provide a possible explanation for the failures of anti-EGFR therapy in GBM and suggest a new approach to the treatment of EGFR-expressing GBM using a combination of EGFR and TNF inhibition.

The identification of genetic abnormalities that are specific to cancer cells has made it possible to develop targeted treatments. The EGFR is a prime target in this therapeutic approach, since it is overexpressed in many types of cancers and may be a key driver of the malignant phenotype. An exciting development in recent years was the identification of EGFR activating mutations in a subset of lung cancers, which render cells harboring such mutations oncogene addicted and very sensitive to the effects of EGFR tyrosine kinase inhibitors (TKIs)[1,2]. However, the inevitable development of secondary resistance has limited the effectiveness of EGFR inhibition in lung cancer. The development of secondary resistance in lung cancer has spurred intensive investigation into mechanisms of EGFR TKI resistance and resulted in important insights into secondary resistance to EGFR TKIs in lung cancer. The main mechanisms identified in lung cancer include the emergence of EGFR mutations such as the T790M mutation and activation of other receptor tyrosine kinases, such as Met or Axl, that confer resistance to EGFR TKIs[3]. In addition to genetic and delayed mechanisms, rapid feedback loops with activation of STAT3 (signal transducer and activator of transcription 3) have also been invoked to mediated EGFR TKI resistance in lung cancer cells with EGFR activating mutations[4,5]. However, most EGFR-expressing tumors in both the lung and the brain do not appear to be oncogene addicted, and EGFR TKIs, so far, have not been effective in such cancers.

EGFR gene amplification and increased EGFR expression are detected in 40–50% of GBMs, the most common primary malignant adult brain tumor[6,7]. EGFRvIII is the most common oncogenic EGFR mutant in GBM and may be more sensitive to EGFR inhibition[8]. There has been a substantial, and thus far unsuccessful, effort to inhibit the EGFR as a therapeutic strategy in GBM[9]. While not much is known about what mediates primary resistance to EGFR inhibition in GBMs expressing EGFR wild type (EGFRwt), a number of studies have provided key insights into mechanisms that mediate secondary resistance to EGFR inhibitors such as erlotinib in EGFRvIII-expressing glioma cells after an initial period of responsiveness. For example, prolonged EGFR inhibition leads to an increased expression of platelet-derived growth factor receptor-β (PDGFRβ) that mediates a secondary resistance to erlotinib[10]. Another study demonstrated that secondary resistance to erlotinib in GBM is mediated via a dynamic downregulation of EGFRvIII[11]. A comparison of erlotinib sensitivity in EGFR lung cancer mutations versus the EGFRvIII mutation suggested that EGFRvIII-containing cancers are resistant to erlotinib because of lower kinase-site occupancy and more rapid cycling of erlotinib[12]. Another study identified a urokinase receptor–Bim signaling axis as mediating EGFR inhibitor resistance[13].

Primary resistance to EGFR inhibition in cancer cells expressing EGFRwt or resistant EGFR mutants may occur because the EGFR does not drive survival or proliferation of these cells or because adaptive signals prevent cell death. If primary resistance is mediated via an early adaptive response, there is the possibility of inhibiting this adaptive response and overcoming primary resistance to EGFR

[1]Department of Neurology and Neurotherapeutics, University of Texas Southwestern Medical Center, Dallas, Texas, USA. [2]Department of Pathology, University of Texas Southwestern Medical Center, Dallas, Texas, USA. [3]Department of Neurosurgery, University of Texas Southwestern Medical Center, Dallas, Texas, USA. [4]Department of Radiation Oncology, University of Texas Southwestern Medical Center, Dallas, Texas, USA. [5]Department of Internal Medicine, University of Texas Southwestern Medical Center, Dallas, Texas, USA. [6]Veterans Affairs North Texas Health Care System, Dallas, Texas, USA. [7]Department of Translational Neuro-Oncology and Neurotherapeutics, John Wayne Cancer Institute at Providence Saint John's Health Center, Santa Monica, California, USA. [8]Department of Radiation Oncology, Mayo Clinic, Rochester, Minnesota, USA. [9]Departments of Biomedical Engineering and Cancer Biology, Wake Forest School of Medicine, Winston-Salem, North Carolina, USA. Correspondence should be addressed to A.A.H. (amyn.habib@utsouthwestern.edu).

inhibition. Here we show that primary resistance in EGFR-expressing glioma cells is mediated by a rapid adaptive signaling pathway that is triggered by inhibition of EGFRwt or mutant EGFR. We propose that a TNF–JNK–Axl–ERK signaling pathway mediates this adaptive response. Inhibition of this pathway in EGFR-expressing glioma cells confers sensitivity to EGFR inhibition in cell culture, as well as in a mouse model.

RESULTS

Erlotinib induces a feedback activation of ERK in glioma cells

To elucidate mechanisms of EGFR inhibition resistance in glioma cells, we examined signal transduction events following erlotinib exposure in glioma cells. We used EGFR-expressing patient-derived primary GBM neurospheres, as well as established glioblastoma cell lines expressing EGFRwt or EGFRvIII (**Fig. 1a**). Signaling from EGFRvIII is constitutive, while signaling from overexpressed EGFRwt may be constitutive or ligand induced[7,14–19]. Primary GBM neurospheres GBM9, GBM39 and SK987 express EGFRvIII and also EGFRwt and have been described previously[20–23]. We started our investigation by examining activation of the serine/threonine kinase Akt, STAT3 and ERK, since these pathways are important in cancer

cell survival. Upon exposure of GBM9 neurospheres to erlotinib, the ERK activation present in untreated cells decreased after addition of erlotinib, suggesting that EGFR was driving the activation of ERK. A reactivation of ERK was seen at 24–48 h in erlotinib-treated cells, likely triggered by a feedback mechanism, since the EGFR remained inactivated (**Fig. 1b**). However, we did not detect an increase in Akt or STAT3 activation (**Fig. 1b**). Similar results were obtained in patient-derived primary GBM39 and SK987 neurospheres (**Fig. 1c,d**). We also examined signal transduction in established glioblastoma cell lines U87EGFRwt, U87EGFRvIII and U251EGFRwt and found a similar feedback activation of ERK in response to EGFR inhibition (**Fig. 1e,f** and **Supplementary Fig. 1a**). Similar results were also obtained with afatinib, an irreversible direct inhibitor of EGFR kinase activity (**Supplementary Fig. 1b**). When we used a higher concentration of erlotinib, STAT3 and Akt activation were suppressed. However, we did not detect any reactivation of STAT3 or Akt in the presence of continuing EGFR inhibition (**Supplementary Fig. 1c–g**). Thus, of the three pathways examined, only ERK became activated in response to EGFR inhibition. In U87EGFRwt cells, ERK and EGFR activation were similar in serum or serum-free conditions (**Supplementary Fig. 1h**). Basal EGFR and ERK activation could be inhibited by cetuximab,
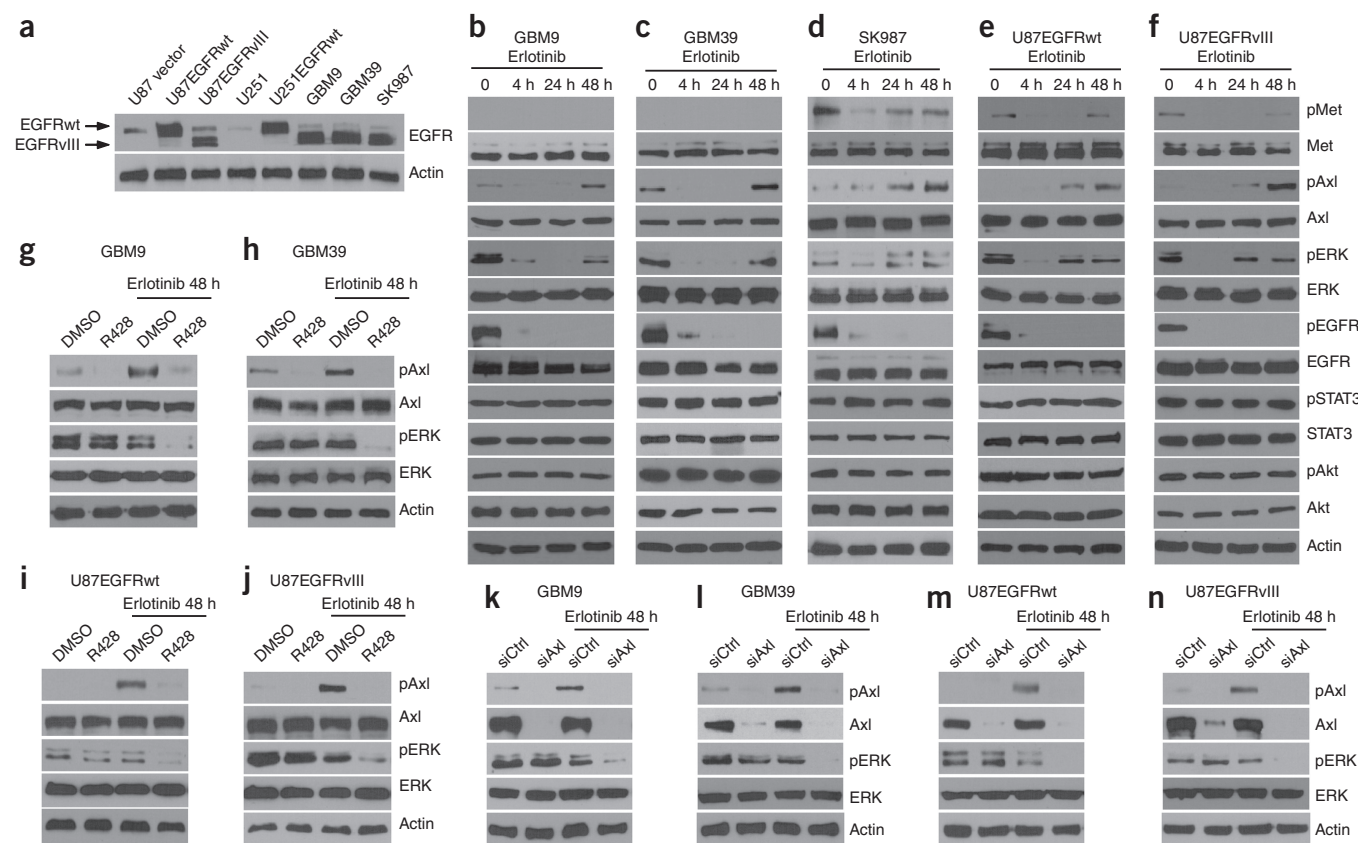

Figure 1 EGFR inhibition triggers an adaptive response in glioma cells. (**a**) Western blot showing EGFR levels in established GBM cell lines and patient-derived primary GBM neurospheres. U87 vector indicates U87MG cells transfected with an empty vector. U251 is an established GBM cell line. β-actin was used as a loading control. (**b**) Patient-derived primary GBM neurospheres (GBM9) were exposed to erlotinib (1 μM) for the indicated times followed by western blot with the indicated antibodies; pMet, pAxl, pERK, pEGFR, pSTAT3 and pAkt specifically detect phosphorylated isoforms. (**c,d**) A similar experiment in GBM neurospheres derived from two different patients (GBM39 and SK987). (**e**) U87EGFR cells were treated with erlotinib (1 μM) for the indicated times followed by western blot with the indicated antibodies. (**f**) A similar experiment was conducted in U87EGFRvIII cells. (**g–j**) Axl was inhibited using the specific inhibitor R428 (1 μM). Cells were exposed to erlotinib followed by western blot. Erlotinib-induced ERK activation is inhibited when the Axl inhibitor is used in both established GBM cell lines and patient-derived neurospheres. (**k–n**) siRNA knockdown of Axl results in an inhibition of erlotinib-induced ERK activation in both established cell lines and patient-derived neurospheres. Control siRNA or Axl siRNA was transfected into cells (for 48 h), followed by addition of erlotinib for 48 h and western blot with indicated antibodies. Western blots shown in **a–n** are representative of at least three independent replicates. Full-length blots are presented in **Supplementary Figure 11**.
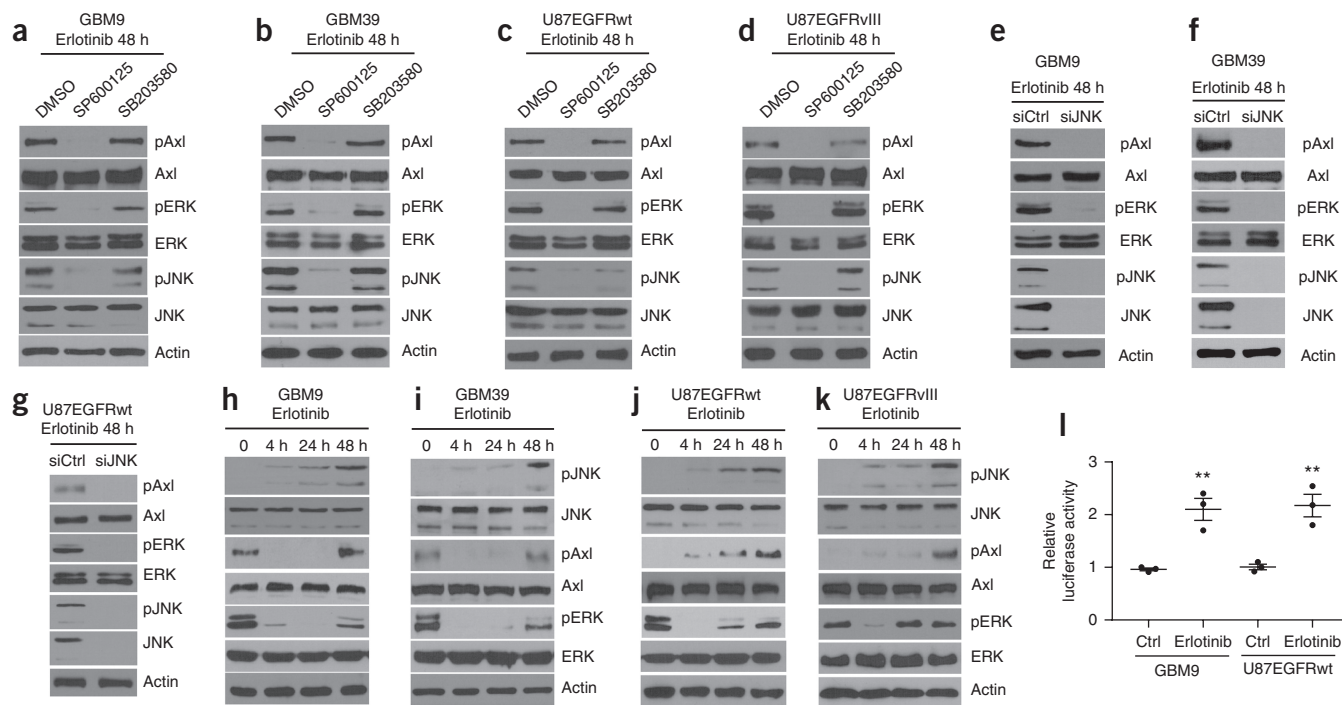
Figure 2 EGFR inhibition–induced Axl and ERK activation is mediated by JNK. (**a,b**) Patient-derived primary GBM neurospheres were exposed to erlotinib for 48 h in the presence or absence of the JNK inhibitor SP600125 (1 μM) or p38 inhibitor SB203580 (10 μM), followed by western blot with the indicated antibodies. DMSO indicates vehicle alone. (**c,d**) U87EGFRwt or U87EGFRvIII cells were exposed to erlotinib for 48 h in the presence or absence of SP600125 or SB203580, followed by western blot with the indicated antibodies. (**e,f**) siRNA knockdown for JNK1 and JNK2 (siJNK) was conducted in GBM9 and GBM39 neurospheres, followed by exposure to erlotinib for 48 h and western blot with the indicated antibodies. siCtrl indicates scrambled control siRNA. (**g**) A similar experiment was done in U87EGFRwt cells. (**h–k**) JNK is activated in response to erlotinib in patient-derived primary neurospheres, as well as in established GBM cell lines, as determined by the phosphorylation of JNK. Western blots shown in **a–k** are representative of at least three independent replicates. Full-length blots are presented in **Supplementary Figure 12**. (**l**) A luciferase reporter assay shows that EGFR inhibition with erlotinib results in an increase in AP-1 transcriptional activity in GBM9 and U87EGFRwt cells. Erlotinib was used for 24 h (1 μM). DMSO was used as a control (Ctrl). GBM9: Ctrl versus erlotinib: $P = 0.0056$, $t = 5.43$, d.f. = 4, $**P < 0.01$; U87EGFRwt: Ctrl versus erlotinib: $P = 0.0061$, $t = 5.31$, d.f. = 4, $**P < 0.01$. Data are presented as mean ± s.e.m. Significant difference analyzed by an unpaired Student's t-test ($n = 3$ biologically independent experimental replicates).

which blocks binding of ligand to the EGFR, suggesting autocrine activation of EGFR under serum-starved conditions (**Supplementary Fig. 1i**). As expected, further increases in EGFR and ERK activation were detected when exogenous epidermal growth factor (EGF) was added (**Supplementary Fig. 1j**).

Inhibition of Axl blocks EGFR inhibition mediated ERK activation

Activation of other receptor tyrosine kinases such as Met or Axl has been identified as a major mechanism of secondary resistance to EGFR inhibition in lung cancer cells. In glioma, EGFRvIII expression leads to coactivation of multiple receptor tyrosine kinases, such as Met, and a combined inhibition of EGFR and Met or of Akt and the mechanistic target of rapamycin (mTOR) is more effective than inhibition of the EGFR alone[24–29]. Increased expression of PDGFRβ has been described in response to prolonged EGFR inhibition in glioma cells[10]. We detected phosphorylation of the receptor tyrosine kinase Axl following exposure of cells to erlotinib for 48 h in patient-derived GBM neurospheres and in all cell lines examined (**Fig. 1b–f** and **Supplementary Fig. 1a**). Erlotinib also induced activation of Met in established cell lines, but in only one patient-derived neurosphere, SK987 (**Fig. 1b–f** and **Supplementary Fig. 1a**). Since Axl activation was seen in all patient-derived neurospheres and established cell lines tested, we focused on Axl in this study.

We next examined whether Axl was responsible for activation of ERK in response to EGFR inhibition. We used the Axl inhibitor

R428 and found that inhibition of Axl resulted in a block of erlotinib-induced ERK activation in patient-derived GBM neurospheres, as well as in multiple cell lines (**Fig. 1g–j**). Similarly, short interfering RNA (siRNA) knockdown of Axl also resulted in a block of erlotinib-induced ERK activation (**Fig. 1k–n**). Thus, Axl is essential to EGFR-induced inhibition of ERK activation.

Activation of JNK by EGFR inhibition triggers a survival feedback loop

We next examined whether inhibition of key signaling pathways known to be active in EGFR signaling could block erlotinib-induced Axl and ERK activation. We found that the JNK inhibitor SP600125 inhibited erlotinib-induced activation of Axl and ERK in patient-derived neurospheres and in established GBM cell lines, but the p38 mitogen-associated protein kinase (MAPK) inhibitor SB203580 failed to do so (**Fig. 2a–d**). We also found that siRNA knockdown of JNK1 and JNK2 resulted in a block of erlotinib-induced EGFR Axl and ERK activation (**Fig. 2e–g**). Furthermore, erlotinib exposure of cells resulted in activation of JNK as detected by phosphorylation of JNK in western blots (**Fig. 2 h–k**). These findings suggest that JNK activation is essential to erlotinib-induced ERK activation. JNK proteins are MAPKs that phosphorylate c-Jun. This results in activation of the transcription factor AP-1. Consistent with data demonstrating JNK activation in response to EGFR inhibition, erlotinib also induced increased activity of the AP-1 reporter (**Fig. 2l**). These experiments
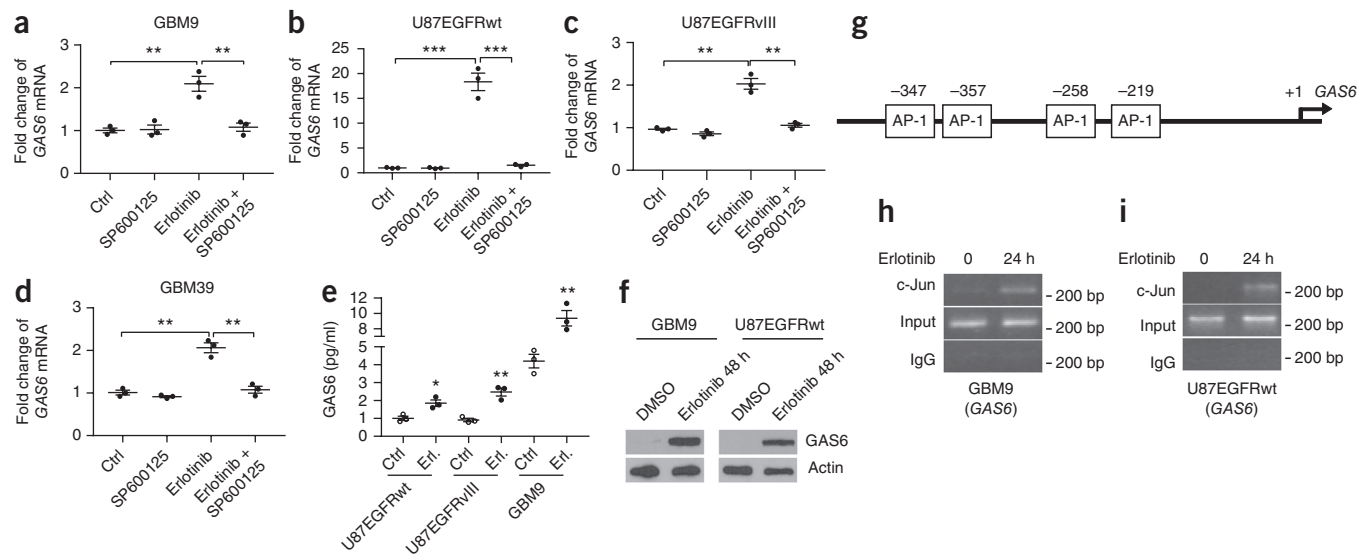
Figure 3 EGFR inhibition leads to an increase in GAS6 via a JNK-dependent mechanism. (**a**) GBM9 neurospheres were exposed to erlotinib in the absence or presence of the JNK inhibitor SP600125 (1 µM) for 24 h, followed by quantitative real-time PCR for *GAS6* mRNA. DMSO was used as a control (Ctrl). *GAS6* is increased upon EGFR inhibition, and this increase is blocked by JNK inhibition. Ctrl versus erlotinib: $P = 0.0039$, $t = 5.98$, d.f. = 4; erlotinib versus erlotinib + SP600125: $P = 0.0070$, $t = 5.10$, d.f. = 4. (**b**–**d**) A similar experiment was undertaken in U87EGFRwt, U87EGFRvIII and patient-derived GBM39 neurospheres. (**b**) Ctrl versus erlotinib: $P = 0.0006$, $t = 9.83$, d.f. = 4; erlotinib versus erlotinib + SP600125: $P = 0.0007$, $t = 9.48$, d.f. = 4. (**c**) Ctrl versus erlotinib: $P = 0.0011$, $t = 8.39$, d.f. = 4; erlotinib versus erlotinib + SP600125: $P = 0.0018$, $t = 7.32$, d.f. = 4. (**d**) Ctrl versus erlotinib: $P = 0.0012$, $t = 8.20$, d.f. = 4; erlotinib versus erlotinib + SP600125: $P = 0.0022$, $t = 6.97$, d.f. = 4. (**e**) An ELISA showing the increase in GAS6 protein induced by erlotinib (1 µM for 24 h). U87EGFRwt: Ctrl versus erlotinib (Erl.): $P = 0.0175$, $t = 3.90$, d.f. = 4; U87EGFRvIII: Ctrl versus erlotinib: $P = 0.0030$, $t = 6.45$, d.f. = 4; GBM9: Ctrl versus erlotinib: $P = 0.0087$, $t = 4.80$, d.f. = 4. Data are presented as mean ± s.e.m.; *$P < 0.05$, **$P < 0.01$, ***$P < 0.001$ from two-tailed unpaired Student's t-test ($n = 3$ biologically independent experimental replicates). (**f**) Western blot showing increase in GAS6 protein in both GBM9 and U87EGFRwt cells upon erlotinib treatment. Western blots shown in **a**–**k** are representative of at least three independent replicates. Full-length blots are presented in **Supplementary Figure 12**. (**g**) A schematic of the *GAS6* promoter showing AP-1 sites. (**h**,**i**) ChIP assay showing the presence of c-Jun on the *GAS6* promoter in response to erlotinib (1 µM for 24 h) in GBM9 neurospheres and in U87EGFRwt cells. ChIP results are representative of at least three independent replicates. Full-length DNA agarose gels are presented in **Supplementary Figure 12**.

support a model in which EGFR inhibition leads to the activation of JNK signaling and, in turn, JNK signaling mediates an activation of Axl. Axl activation then leads to ERK activation.

EGFR inhibition has also been reported to result in a rapid activation of NF-κB in lung cancer cells expressing activating EGFR mutations[30]. However, we did not detect an increase in NF-κB transcriptional activity in response to EGFR inhibition in glioma cells, whereas lipopolysaccharide efficiently activated NF-κB transcriptional activity (**Supplementary Fig. 2a**,**b**).

Activation of Axl results from increased expression of GAS6

Next we examined the mechanism of Axl activation following exposure to erlotinib. Axl was activated about 24–48 h after the EGFR was inhibited. We investigated the possibility that erlotinib may lead to increased expression of GAS6, the ligand for Axl. We examined the erlotinib-induced expression of *GAS6* at various time points by real-time quantitative PCR. EGFR inhibition led to an increase in *GAS6* in patient-derived neurospheres and in established GBM cell lines (**Fig. 3a**–**d**). Notably, inhibition of JNK blocked erlotinib-induced expression of *GAS6* (**Fig. 3a**–**d**), consistent with the previously noted inhibition of erlotinib-induced Axl activation by chemical inhibition or silencing of JNK. An increase in GAS6 was confirmed by ELISA and western blot (**Fig. 3e**,**f**). These findings suggest that erlotinib-induced activation of Axl likely results from an increase in GAS6. Next, we examined whether activation of JNK leads to increased transcription of *GAS6*. The TFBIND program identified multiple predicted c-Jun (AP-1) binding sites 500 bp upstream of the putative transcription

start site of *GAS6* (**Fig. 3g**). We then undertook a chromatin immunoprecipitation (ChIP) assay to investigate the presence of AP-1 at the *GAS6* promoter. Erlotinib exposure led to the binding of c-Jun to the *GAS6* promoter in GBM9 and U87EGFRwt cells (**Fig. 3h**,**i**).

JNK is activated by an erlotinib-induced increase in TNF

Next we examined the mechanism of erlotinib-induced JNK activation. Previous studies have found that EGFR inhibition in lung cancer cells results in increased secretion of inflammatory cytokines[5]. We hypothesized that EGFR inhibition in glioma cells may lead to a similar release of cytokines. Since TNF is a known and potent activator of JNK[31], we quantified TNF in patient-derived GBM neurospheres, as well as EGFR-expressing cell lines. Erlotinib led to a significant and rapid increase in *TNF* mRNA, as determined by real-time quantitative PCR (**Fig. 4a**–**d**). The increase in TNF was confirmed at a protein level by ELISA (**Fig. 4e**). The increase in TNF was noted in additional lines and patient-derived neurospheres (**Supplementary Fig. 2c**,**d**). Notably, an increase in TNF was also induced by EGFR inhibition in tumors growing in mice (**Fig. 4f**). In this experiment, patient-derived primary GBM9 cells were injected into the flanks of athymic mice. After formation of a palpable tumor, erlotinib was administered as indicated, followed by collection of tumors and ELISA for TNF. An erlotinib-induced increase in TNF was detected 1 d after administration of erlotinib (**Fig. 4f**). In addition, we also detect erlotinib-induced activation of JNK, Axl and ERK in mouse tumors (**Fig. 4g**), peaking around 2–7 d and subsiding by 14 d.

Next we examined whether TNF is essential role in erlotinib-induced JNK activation. We indeed found that a neutralizing antibody
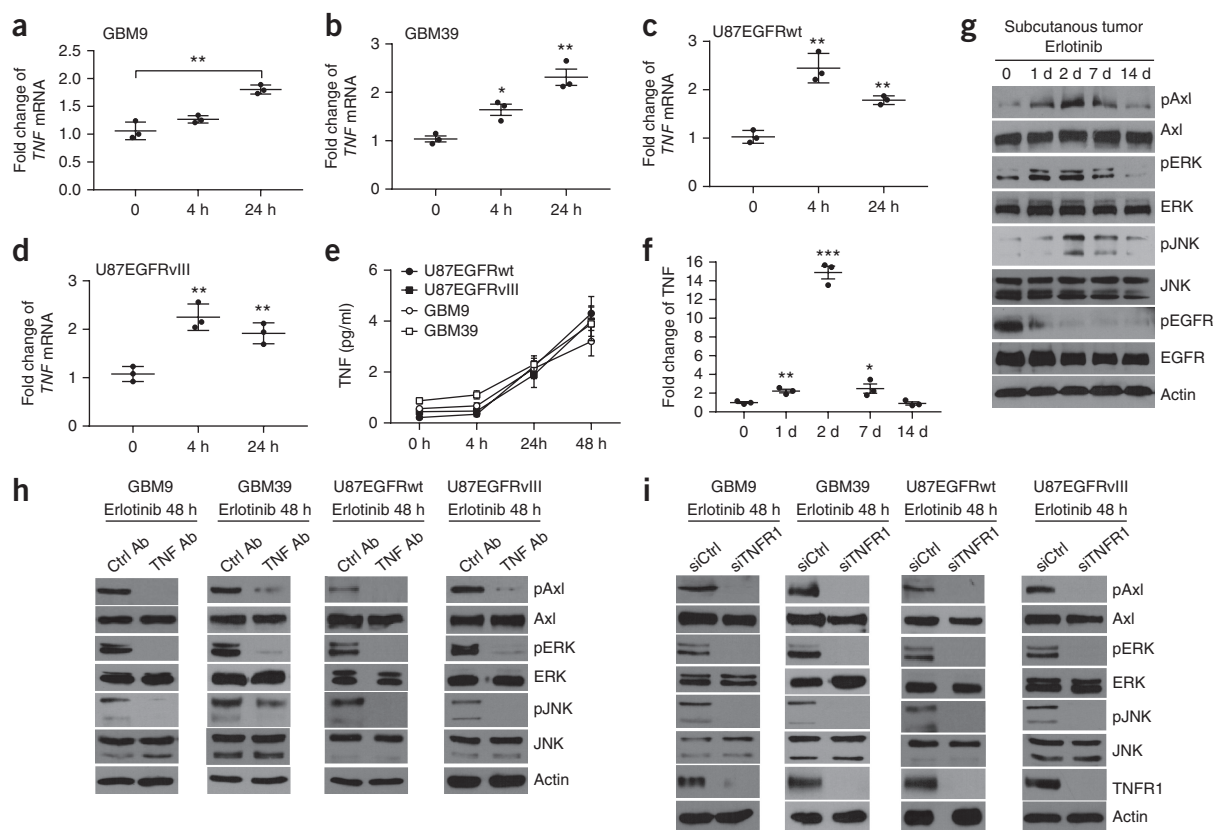
Figure 4 EGFR inhibition leads to increased TNF signaling that triggers an adaptive signaling pathway. (**a**,**b**) EGFR inhibition leads to an increase in *TNF* mRNA in patient-derived GBM9 and GBM39 neurospheres. Cells were exposed to erlotinib (100 nM) for the times indicated followed by real-time quantitative PCR for *TNF* mRNA. (**a**) 0 versus 24 h: $P = 0.0019$, $t = 7.22$, d.f. = 4. (**b**) 0 versus 4 h: $P = 0.0102$, $t = 4.58$, d.f. = 4; 0 versus 24 h: $P = 0.0021$, $t = 7.10$, d.f. = 4. (**c**,**d**) A similar experiment was conducted in U87EGFRwt and U87EGFRvIII cells using an erlotinib concentration of 1 μM. (**c**) 0 versus 4 h: $P = 0.0018$, $t = 7.41$, d.f. = 4; 0 versus 24 h: $P = 0.0012$, $t = 8.20$, d.f. = 4. (**d**) 0 versus 4 h: $P = 0.0030$, $t = 6.46$, d.f. = 4; 0 versus 24 h: $P = 0.0054$, $t = 5.47$, d.f. = 4. (**e**) A TNF ELISA was performed on supernatants from erlotinib treated U87EGFRwt and U87EGFRvIII cells (1 μM) and GBM9 and GBM39 neurospheres (100 nM). U87EGFRwt: 0 versus 24 h: $P = 0.0056$, $t = 5.42$, d.f. = 4; 0 versus 48 h: $P = 0.0006$, $t = 10.4$, d.f. = 4; U87EGFRVIII: 0 versus 24 h: $P = 0.0022$, $t = 6.98$, d.f. = 4; 0 versus 48 h: $P = 0.0083$, $t = 4.86$, d.f. = 4; GBM9: 0 versus 24 h: $P = 0.01$, $t = 4.6$, d.f. = 4; 0 versus 48 h: $P = 0.0043$, $t = 5.84$, d.f. = 4; GBM39: 0 versus 24 h: $P = 0.0189$, $t = 3.82$, d.f. = 4; 0 versus 48 h: $P = 0.0024$, $t = 6.81$, d.f. = 4. Data are presented as mean ± s.e.m.; *$P < 0.05$, **$P < 0.01$, ***$P < 0.001$ from two-tailed unpaired Student's *t*-test ($n = 3$ biologically independent experimental replicates). (**f**) Time course of TNF upregulation in mouse tumors exposed to erlotinib 50 mg/kg for the indicated time points after formation of subcutaneous tumors ($n = 3$). Tumors were removed after erlotinib exposure, followed by TNF ELISA on protein extracts. 0 versus 1 d: $P = 0.0045$, $t = 5.77$, d.f. = 4; 0 versus 2 d: $P = 0.0002$, $t = 13.92$, d.f. = 4; 0 versus 7 d: $P = 0.0245$, $t = 3.52$, d.f. = 4. Data are presented as mean ± s.e.m.; *$P < 0.05$, **$P < 0.01$, ***$P < 0.001$ from two-tailed unpaired Student's *t*-test. (**g**) Signal transduction in tumors exposed to erlotinib (50 mg/kg) for the indicated time points. (**h**) A neutralizing antibody to TNF (TNF Ab) (2 μg/ml) blocked erlotinib-induced activation of Axl, ERK and JNK in GBM9 and GBM39 neurospheres and U87EGFRwt and U87EGFRvIII cell lines, while control antibody (Ctrl Ab) had no effect. The control antibody was normal mouse IgG. (**i**) siRNA knockdown of TNFR1 (siTNFR1) blocked erlotinib-induced activation of Axl, ERK and JNK in GBM9 and GBM39 neurospheres and in U87EGFRwt and U87EGFRvIII cell lines, while control (scrambled) siRNA (siCtrl) had no effect. Western blots shown in **g**–**i** are representative of at least three independent replicates. Full-length blots are presented in **Supplementary Figure 13**.

to TNF led to inhibition of erlotinib-induced JNK activation (**Fig. 4h**). Furthermore, erlotinib-induced Axl and ERK activation were also blocked by TNF inhibition. Similar results were found with siRNA knockdown of TNF receptor 1 (TNFR1) (**Fig. 4i**). We also examined levels of TNFR1 in glioma cells treated with erlotinib. Erlotinib induced a downregulation of TNFR1 in patient-derived samples and established GBM cell lines (**Supplementary Fig. 2e**). As TNF induces downregulation of its receptor[32], this finding provides evidence that TNF signaling is activated by EGFR inhibition.

Inhibition of the TNF–JNK–Axl–ERK axis confers erlotinib sensitivity on EGFR-expressing glioma cells
To investigate whether this TNF–JNK–Axl–ERK signaling pathway influences the biological response to EGFR inhibition, we examined

the effect of inhibiting this pathway on the viability of glioma cells exposed to erlotinib. First we examined the sensitivity of EGFR-expressing GBM cell lines to erlotinib. The established cell lines appeared to be completely resistant to erlotinib regardless of whether EGFRwt or EGFRvIII is expressed (**Fig. 5a**). Patient-derived primary neurosphere GBM9 and GBM39 cells were resistant to EGFR inhibition at a low concentration of erlotinib (100 nM). However, when combined with JNK inhibition using SP600125 or ERK inhibition using U0126, erlotinib led to substantial cell death, although cells were resistant to JNK or ERK inhibition alone (**Fig. 5b,c**). Inhibitors of several other signaling pathways failed to sensitize glioma cells to EGFR inhibition (**Supplementary Fig. 2f**). Established glioblastoma cell lines were also resistant to EGFR inhibition or JNK inhibition or ERK inhibition alone, but a combined inhibition of EGFR with ERK
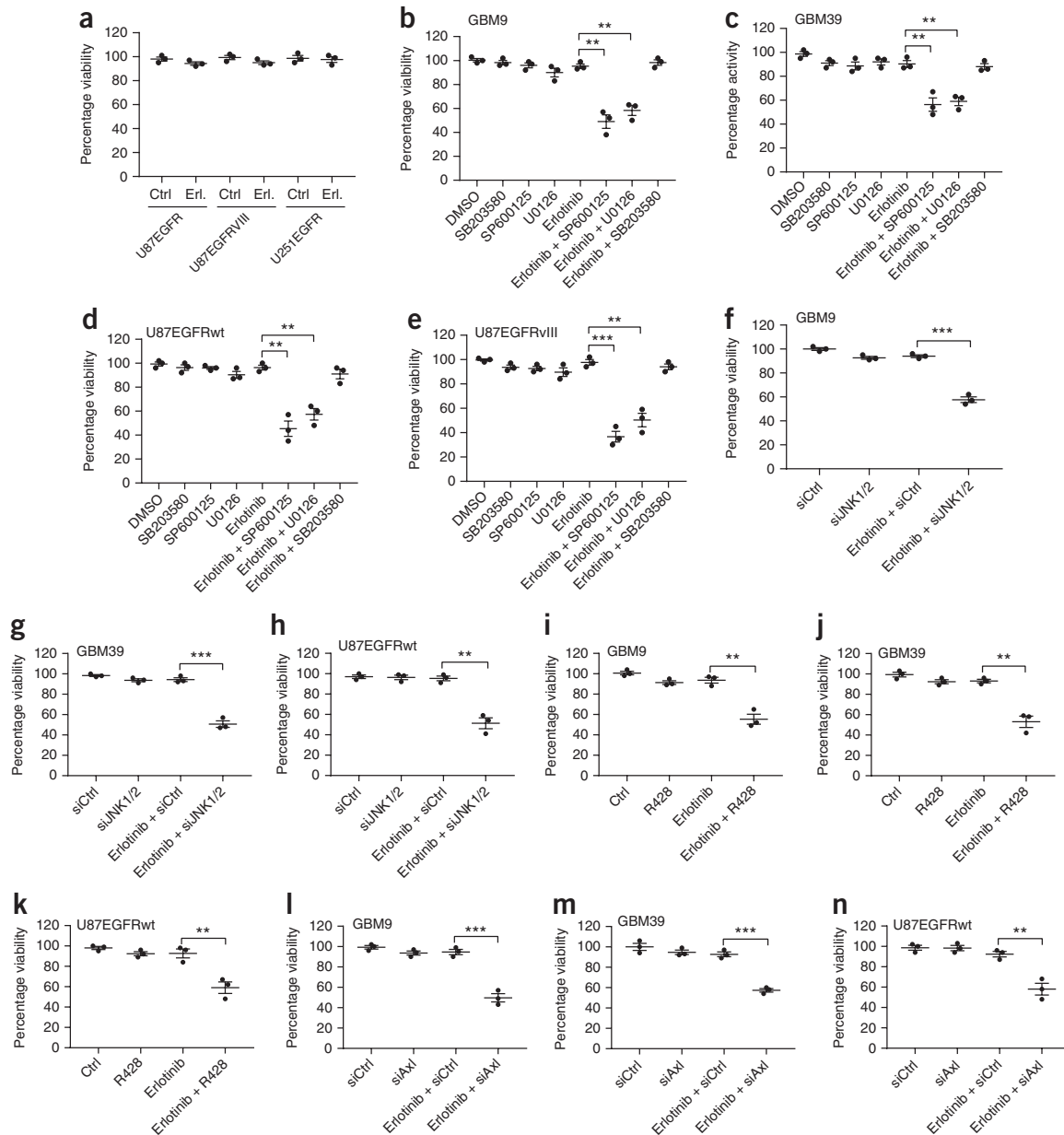
Figure 5 Inhibition of JNK and ERK renders glioma cells sensitive to EGFR inhibition. (**a**) AlamarBlue assay in established GBM cell lines exposed to erlotinib (Erl.; 10 µM). Cells are completely resistant to the effects of EGFR inhibition. DMSO was used as a control (Ctrl). (**b**,**c**) Patient-derived GBM9 or GBM39 neurospheres were exposed to erlotinib (100 nM) with or without the JNK inhibitor SP600125 (1 µM), p38 inhibitor SB203580 (10 µM) or ERK inhibitor U0126 (1 µM), followed by AlamarBlue cell survival assay after 72 h of inhibitor exposure. (**b**) Erlotinib versus erlotinib + SP600125: $P = 0.0015$, $t = 7.75$, d.f. = 4; erlotinib versus erlotinib + U0126: $P = 0.0013$, $t = 8.10$, d.f. = 4. DMSO indicates vehicle alone. (**c**) Erlotinib versus erlotinib + SP600125: $P = 0.0057$, $t = 5.41$, d.f. = 4; erlotinib versus erlotinib + U0126: $P = 0.0023$, $t = 6.93$, d.f. = 4. (**d**,**e**) A similar experiment conducted in U87EGFRwt and U87EGFRvIII cells. (**d**) Erlotinib versus erlotinib + SP600125: $P = 0.0016$, $t = 7.61$, d.f. = 4; erlotinib versus erlotinib + U0126: $P = 0.0017$, $t = 7.48$, d.f. = 4. (**e**) Erlotinib versus erlotinib + SP600125: $P = 0.0003$, $t = 12.23$, d.f. = 4; erlotinib versus erlotinib + U0126: $P = 0.0014$, $t = 7.87$, d.f. = 4. (**f**) siRNA knockdown of JNK1 and JNK2 (siJNK1/2) in GBM9 neurospheres results in an enhanced sensitivity to erlotinib, whereas scrambled control siRNA (siCtrl) has no effect. Erlotinib + siCtrl versus erlotinib + siJNK1/2: $P = 0.0002$, $t = 13.96$, d.f. = 4. (**g**) siRNA knockdown of JNK1 and JNK2 in GBM39 neurosphere cells has a similar effect. Erlotinib + siCtrl versus erlotinib + siJNK1/2: $P = 0.0003$, $t = 11.86$, d.f. = 4. (**h**) siRNA knockdown of JNK1 and JNK2 in U87EGFRwt cells results in an enhanced sensitivity to erlotinib, whereas control siRNA has no effect. Erlotinib + siCtrl versus erlotinib + siJNK1/2: $P = 0.0017$, $t = 7.52$, d.f. = 4. (**i**,**j**) Patient-derived GBM9 or GBM39 neurospheres were exposed to erlotinib (100 nM) with or without the Axl inhibitor R428 (1 µM) followed by AlamarBlue cell survival assay after 72 h. (**i**) Erlotinib versus erlotinib + R428: $P = 0.0025$, $t = 6.75$, d.f. = 4. (**i**) Erlotinib versus erlotinib + R428: $P = 0.0023$, $t = 6.93$, d.f. = 4. (**k**) A similar experiment was done in U87EGFRwt cells using an erlotinib concentration of 1 µM. Erlotinib versus erlotinib + R428: $P = 0.0094$, $t = 4.69$, d.f. = 4. (**l**–**n**) siRNA knockdown of Axl (siAxl) in GBM9 and GBM39 neurospheres or U87EGFRwt cells sensitizes cells to the effect of erlotinib as determined by AlamarBlue cell viability assay, but scrambled control siRNA does not. (**l**) Erlotinib + siCtrl versus erlotinib + siAxl: $P = 0.0004$, $t = 11.23$, d.f. = 4. (**m**) Erlotinib + siCtrl versus erlotinib + siAxl: $P = 0.0003$, $t = 12.80$, d.f. = 4. (**n**) Erlotinib + siCtrl versus erlotinib + R428: $P = 0.0058$, $t = 5.38$, d.f. = 4. Data are presented as mean ± s.e.m.; **$P < 0.01$, ***$P < 0.001$ from two-tailed unpaired Student's t-test ($n = 3$ biologically independent experimental replicates).
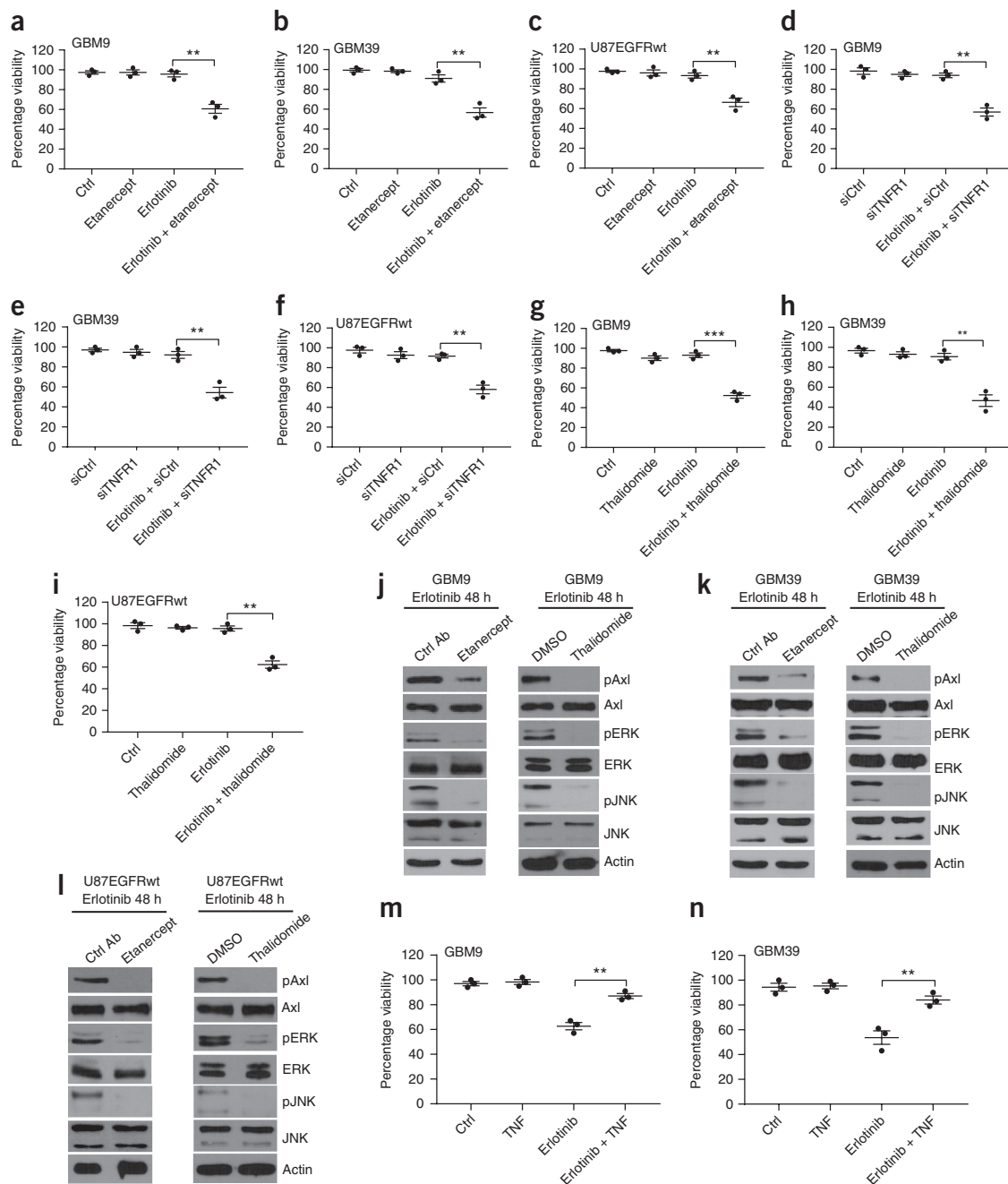
Figure 6 TNF inhibition sensitizes glioma cells to EGFR inhibition. (**a,b**) AlamarBlue cell viability assay in GBM9 or GBM39 neurospheres. Etanercept (100 nM) sensitizes cells to EGFR inhibition with erlotinib. Etanercept and erlotinib were added to GBM9 or GBM39 neurospheres concurrently and AlamarBlue assay was done after 72 h. DMSO was used as a control. (**a**) Erlotinib versus erlotinib + etanercept: $P = 0.0027$, $t = 6.59$, d.f. = 4. (**b**) Erlotinib versus erlotinib + etanercept: $P = 0.0044$, $t = 6.59$, d.f. = 4. (**c**) A similar experiment was performed in U87EGFRwt cells. Erlotinib versus erlotinib + etanercept: $P = 0.0056$, $t = 5.41$, d.f. = 4. (**d,e**) TNFR1 was silenced using siRNA (siTNFR1) in GBM9 and GBM39 cells and cells were exposed to erlotinib for 72 h in stem cell medium without EGF for 72 h, followed by AlamarBlue assay. (**d**) Erlotinib + scrambled control siRNA (siCtrl) versus erlotinib + siTNFR1: $P = 0.0014$, $t = 7.95$, d.f. = 4. (**e**) Erlotinib + siCtrl versus erlotinib + siTNFR1: $P = 0.0041$, $t = 5.90$, d.f. = 4. (**f**) A similar experiment was done in U87EGFRwt cells. Erlotinib + siCtrl versus erlotinib + siTNFR1: $P = 0.0021$, $t = 7.11$, d.f. = 4. (**g–i**) Thalidomide sensitizes GBM9 and GBM39 cells to EGFR inhibition with erlotinib. Thalidomide (1 μM) and erlotinib were added to GBM9 and GBM39 neurospheres (100 nM) or U87EGFRwt cells (1 μM) concurrently and AlamarBlue assay was done after 72 h. (**g**) Erlotinib versus erlotinib + thalidomide: $P = 0.0030$, $t = 6.42$, d.f. = 4. (**h**) Erlotinib versus erlotinib + thalidomide: $P = 0.0027$, $t = 6.59$, d.f. = 4. (**i**) Erlotinib versus erlotinib + thalidomide: $P = 0.0013$, $t = 8.11$, d.f. = 4. (**j,k**) Etanercept or thalidomide blocks erlotinib-induced activation of JNK, Axl and ERK in GBM9 and GBM39 neurospheres, as shown by western blot. Control antibody (Ctrl Ab) is normal mouse IgG. (**l**) A similar experiment was conducted in U87EGFRwt cells. Western blots shown in **j**–**l** are representative of at least three independent replicates. Full-length blots are presented in **Supplementary Figure 14**. (**m,n**) Exogenous TNF protects GBM9 and GBM39 neurospheres from erlotinib-induced cell death. TNF (1 ng/ml) and erlotinib (1 μM) were added to cells concurrently and AlamarBlue cell viability assay was done after 72 h. (**m**) Erlotinib versus erlotinib + TNF: $P = 0.0018$, $t = 7.41$, d.f. = 4. (**n**) Erlotinib versus erlotinib + TNF: $P = 0.0087$, $t = 4.79$, d.f. = 4. Data are presented as mean ± s.e.m.; $**P < 0.01$, $***P < 0.001$ from two-tailed unpaired Student's t-test ($n = 3$ biologically independent experimental replicates).
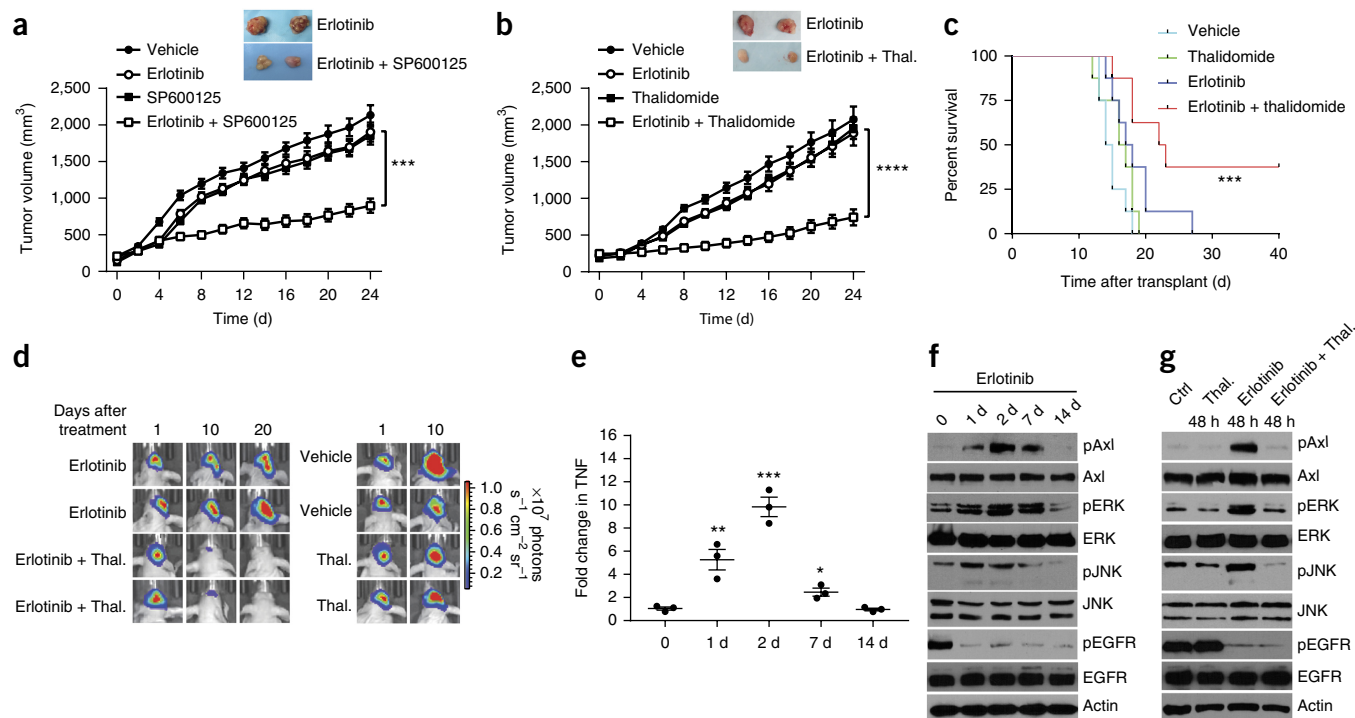
Figure 7 JNK or TNF inhibition sensitizes mouse tumors to EGFR inhibition *in vivo*. (**a**) Treatment of subcutaneous tumors with a combination of erlotinib and SP600125. The tumor growth did not decrease in mice treated with erlotinib or SP600125 alone, whereas the combination of erlotinib and SP600125 decreased tumor growth significantly. Unpaired *t*-test, erlotinib versus erlotinib + SP600125: $P = 0.0003$, $t = 4.70$, d.f. = 14, ***$P < 0.001$. (**b**) Treatment of subcutaneous tumors with a combination of erlotinib and thalidomide. The tumor growth did not decrease in mice treated erlotinib (50 mg/kg) or thalidomide (Thal.; 150 mg/kg) alone, whereas the combination of erlotinib and thalidomide decreased tumor growth significantly. Unpaired *t*-test, erlotinib versus erlotinib + thalidomide: ****$P < 0.0001$, $t = 6.1$, d.f. = 14. (**c**) Combined treatment of erlotinib and thalidomide prolonged survival and suppressed tumor growth in an orthotopic model. Kaplan–Meier survival curves were calculated using GraphPad Prism 7. Statistical significance verified by the log rank test, $P = 0.0008$, ***$P < 0.001$. (**d**) Representative bioluminescence images from erlotinib and erlotinib plus thalidomide groups at days 1, 10 and 20 after treatment. Since all mice in the vehicle and thalidomide groups died within 20 d after transplant, images at day 20 were not available. (**e**) Time course of TNF upregulation in mouse tumors exposed to erlotinib 50 mg/kg for the indicated time points ($n = 3$). Tumors were removed after erlotinib exposure, followed by TNF ELISA on protein extracts. 0 versus 1 d: $P = 0.0091$, $t = 4.73$, d.f. = 4; 0 versus 2 d: $P = 0.0005$, $t = 10.36$, d.f. = 4; 0 versus 7 d: $P = 0.0181$, $t = 3.86$, d.f. = 4. Data are presented as mean ± s.e.m.; *$P < 0.05$, **$P < 0.01$, ***$P < 0.001$ from a two-tailed unpaired Student's *t*-test. (**f**) Signal transduction in intracranial tumors exposed to erlotinib (50 mg/kg) for the indicated time points. (**g**) Western blots of intracranial tumor lysates obtained from erlotinib and/or thalidomide treated mice. Animals without treatment were considered as control (Ctrl, day 0 treatment). Western blots shown in **f** and **g** are representative of three independent replicates. Full-length blots are presented in **Supplementary Figure 14**.

or JNK led to substantial cell death (**Fig. 5d,e**). Biological inhibition of JNK using siRNA knockdown also rendered glioma cells sensitive to EGFR inhibition (**Fig. 5f–h** and **Supplementary Fig. 2g**).

Next we examined whether inhibition of Axl would also render resistant glioma cells sensitive to EGFR inhibition, since Axl inhibition blocks the erlotinib-induced ERK activation. A specific chemical inhibitor of Axl, R428, indeed rendered patient-derived GBM neurospheres and U87EGFRwt cells sensitive to erlotinib (**Fig. 5i–k**). R428 by itself did not affect the viability of these cells. Axl inhibition also conferred sensitivity to erlotinib in established GBM cell lines (**Fig. 5j**). Similarly, siRNA knockdown of Axl also conferred erlotinib sensitivity on GBM9, GBM39 and U87EGFR cells (**Fig. 5l–n** and **Supplementary Fig. 2h**).

Finally, we examined whether inhibition of TNF signaling could render glioma cells sensitive to erlotinib. Inhibition of TNF signaling with the use of etanercept (Enbrel) indeed rendered patient-derived primary GBM neurospheres, as well as established GBM cell lines, sensitive to the effects of EGFR inhibition (**Fig. 6a–c**). Similarly, siRNA knockdown of TNFR1 also resulted in increased sensitivity of cells to EGFR inhibition (**Fig. 6d–f** and **Supplementary Fig. 2i**). Furthermore, the use of thalidomide, an inhibitor of TNF[33], also had

the same effect (**Fig. 6g–i**). Thalidomide may inhibit other cytokines, and we confirmed that thalidomide did indeed block the erlotinib-induced increase in TNF secretion in glioma cell lines (**Supplementary Fig. 3a,b**). We also confirmed that the use of etanercept or thalidomide resulted in an interruption of the erlotinib-induced activation of the JNK–Axl–ERK signaling pathway (**Fig. 6j–l**). In addition, a neutralizing antibody to TNF also enhanced sensitivity of both patient-derived and established GBM lines to EGFR inhibition (**Supplementary Fig. 3c,d**). Afatinib, an irreversible inhibitor of EGFR kinase, in combination with thalidomide had a similar effect (**Supplementary Fig. 3e,f**). Thus, interruption of the adaptive TNF–JNK–Axl–ERK signaling axis at any node renders resistant glioma cells sensitive to EGFR inhibition.

Conversely, activation of TNF signaling by addition of exogenous TNF resulted in protection from cell death induced by EGFR inhibition in patient-derived primary GBM neurospheres. In this experiment, we used a erlotinib concentration of 1 μM, which induces substantial cell death in these cells. Addition of exogenous TNF protected patient-derived primary GBM9 and GBM39 from cell death induced by EGFR inhibition (**Fig. 6m,n**). We also measured changes in cell viability by flow cytometry for annexin V and caspase 3/7 activation

(**Supplementary Figs. 4**–**7**). Glioma cells underwent apoptotic cell death when erlotinib was used in combination with Axl, JNK, ERK or TNF inhibition. Finally, we examined cell proliferation in a cell counting assay. Erlotinib used in combination with Axl, JNK, ERK or TNF inhibition produced significant ($P < 0.01$) decreases in cell numbers in response to combined inhibition of EGFR and JNK, Axl or ERK (**Supplementary Fig. 8**).

Inhibiting the adaptive response renders primarily resistant glioma cells sensitive in a mouse model

Erlotinib-induced JNK activation appears to orchestrate the adaptive response underlying primary resistance of glioma cells to EGFR inhibition. Thus, we examined the effect of inhibiting JNK in a xenograft model in which we injected patient-derived GBM9 neurospheres into the flanks of athymic mice. Once subcutaneous tumors became visible, we divided the mice into control gavage, erlotinib alone, JNK inhibitor (SP600125) alone or erlotinib + SP600125 groups. Erlotinib was administered to animals by oral gavage (50 mg/kg)[23] for 10 d and SP6001125 was administered[34] at a concentration of 40 mg/kg intraperitoneally daily for 10 d. The combined inhibition of JNK and EGFR strongly inhibited the growth of tumors, whereas SP600125 or erlotinib alone had no significant effect on it (**Fig. 7a**).

Next we examined the effect of a combined inhibition of TNF and EGFR. We used thalidomide to inhibit TNF because thalidomide is known to penetrate the blood-brain barrier and has been previously used in GBM (although not in combination with EGFR inhibition)[35]. The experiment was conducted by injecting patient-derived GBM9 neurospheres in the flanks of athymic mice. Once subcutaneous tumors became visible, the mice were divided into control gavage, erlotinib alone, thalidomide alone or erlotinib + thalidomide groups. Erlotinib was administered to animals by oral gavage (50 mg/kg) daily for 10 d and thalidomide was administered at a concentration of 150 mg/kg intraperitoneally daily for 10 d[34,36]. The combined inhibition of TNF and EGFR strongly inhibited the growth of tumors, whereas thalidomide or erlotinib alone had no significant effect on it (**Fig. 7b**).

Next we undertook an orthotopic experiment in athymic mice. Patient-derived GBM9 cells were implanted intracranially, followed by bioluminescence imaging. As we have described recently, GBM9 neurospheres rapidly form tumors in an intracranial model[20]. When tumors became visible on bioluminescence imaging, the mice were divided into four groups and treated with control, erlotinib alone, thalidomide alone or a combination of erlotinib and thalidomide. While neither erlotinib nor thalidomide alone had a significant effect, the combined treatment resulted in a highly significant improved survival of mice treated with a combination of EGFR and TNF inhibition (**Fig. 7c,d**). We repeated the orthotopic experiment with afatinib, another EGFR inhibitor, with similar results (**Supplementary Fig. 9a,b**). In our animal experiments, erlotinib or afatinib was used in combination with thalidomide or SP600125 for a total of 10 d without appreciable short-term toxicity up to the time the mice were sacrificed. The effects of these interventions on the body weight of mice are shown in **Supplementary Figure 9c**–**f**.

Activation of the JNK–Axl–ERK signaling axis was detectable by western blot in intracranial tumors in mice exposed to erlotinib for various time points (**Fig. 7e,f**). We also examined the effect of therapeutic intervention and found that use of a TNF inhibitor (thalidomide) blocked the EGFR inhibition–induced upregulation of the TNF–JNK–Axl–ERK signaling axis in intracranial tumors. (**Fig. 7g**). The temporal profile of this activation was similar to that noted in the subcutaneous model (**Fig. 4g**) and showed an increased activation of this pathway peaking at 2–7 d and subsiding by 14 d. We also

examined activation of JNK, Axl and ERK by immunohistochemistry (**Supplementary Fig. 10**). The results are consistent with our western blot results and show that EGFR inhibition led to activation of the JNK–Axl–ERK signaling axis and that administration of a TNF inhibitor (thalidomide) blocked activation of this pathway.

DISCUSSION

The main finding in our study is that EGFR inhibition in glioma cells results in triggering of a rapid adaptive response that mediates resistance to EGFR inhibition. If this adaptive response is blocked, glioma cells with primary or intrinsic resistance become sensitive to EGFR inhibition and undergo cell death following cessation of EGFR signaling. Previous studies have shown that inhibition of specific tyrosine kinases or key downstream signals in cancer cells leads to a feedback-mediated escape from pathway inhibition by reprogramming of signaling pathways that frequently leads to a resumption of previously suppressed signals or activation of alternative signals that are functionally similar[37,38]. Thus, the cancer cell tends to maintain homeostasis, and it is likely that such mechanisms are an important contributor to drug resistance. Our study demonstrates that a TNF–JNK–Axl–ERK signaling axis mediating an adaptive response to EGFR inhibition in glioma cells is triggered in response to EGFR inhibition. Inhibition of this adaptive response in combination with EGFR inhibition is effective in treatment of glioma tumors in a mouse model.

EGFR gene amplification and overexpression are found in 40–50% of GBMs, and about half of these tumors express the constitutively active oncogenic mutant EGFRvIII[7,39]. EGFRvIII does not bind ligand and is considered constitutively active, although recent studies have revealed a role of coexpressed EGFRwt in the activation of EGFRvIII[40,41]. Studies have demonstrated that EGFRvIII has a greater oncogenic potential than EGFRwt[39]. Recent studies have provided key insights into EGFRvIII downstream signaling and found STAT3 to be a key downstream signal[41–43]. However, EGFRwt may also be oncogenic in GBM[16]. Activation of EGFRwt may be mediated by coexpression of EGFR ligands in the tumor, and studies have documented the presence of EGFR ligands in GBM[14,18]. In addition, overexpression of EGFRwt may also result in a ligand-independent constitutive signaling[14,15,17,18]. Thus, EGFR signaling is likely to be active in GBM cells that express either constitutively active EGFR mutants or EGFRwt. Furthermore, EGFR signaling in patient-derived primary GBM neurospheres, as well as in established GBM cell lines, appears to influence cell survival, since EGFR inhibition in combination with blockade of the TNF–JNK–Axl–ERK adaptive response resulted in cell death both in patient-derived primary GBM cells and in established GBM cell lines. Inhibition of the TNF–JNK–Axl–ERK axis in the absence of EGFR inhibition had no appreciable effect on GBM cell viability.

Many efforts to inhibit the EGFR have failed in GBM[9], the most recent being the failure of a vaccine against EGFRvIII. The first study of targeted EGFR TKI in GBM involved a single-arm phase II trial of gefitinib at first recurrence. No radiographic responses were noted, and median overall survival was about 39 weeks[44]. Subsequent studies with erlotinib in recurrent GBM were also not effective. Trials of EGFR TKIs in combination with temozolomide and radiation in newly diagnosed GBM have not demonstrated improved outcomes[45,46]. Another treatment strategy involves targeting the EGFRvIII mutation with a vaccine (rindopepimut) consisting of a peptide conjugated to keyhole limpet hemocyanin designed to generate a specific immune response against tumor cells with EGFRvIII mutations. A phase II multicenter trial of rindopepimut in newly diagnosed GBM demonstrated a median overall survival of 21.8 months and a 3-year survival of 26%,

suggesting some early promise of efficacy[47]. However, interim analysis of the subsequent phase III study of rindopepimut plus temozolomide in newly diagnosed GBM (ACT IV) demonstrated no difference in median overall survival compared to temozolomide plus control keyhole limpet hemocyanin injections, and thus the trial was discontinued early (https://clinicaltrials.gov identifier NCT01480479).

The dynamic complexity of the glioblastoma genome poses a formidable challenge to effective treatment. Tumor heterogeneity may also limit the effectiveness of EGFR inhibition[48,49]. We propose that the many failures of anti-EGFR therapy in GBM may have resulted, at least in part, from a rapid adaptive response triggered by an increase in TNF signaling. TNF is a central player in the inflammatory response and also in the pathogenesis of cancer. Depending on the cellular context, TNF signaling may promote cell survival or cell death. Our findings indicate that TNF is the primary mediator of intrinsic resistance to EGFR inhibition and promotes cell survival in response to a loss of EGFR signaling via activation of JNK. JNK, in turn, increases expression of GAS6, a ligand for the Axl receptor. Inhibition of TNF or JNK blocks erlotinib-induced Axl activation. Axl activation, in turn, leads to ERK activation. Interruption of the TNF–JNK–Axl–ERK axis at any node resulted in increased sensitivity to EGFR inhibition. In GBM xenograft tumors, erlotinib induced an upregulation of TNF in about 24 h and TNF levels subsided in about a week, while the JNK–ERK–Axl activation subsided in about 2 weeks. It is thus not feasible to detect EGFR inhibition–induced TNF upregulation or JNK–ERK–Axl activation in archival tissue from patients following erlotinib treatment because tissue is not sampled at early time points after TKI treatment. It is likely that key mechanisms of secondary resistance such as a downregulation of EGFRvIII or upregulation of PDGFRβ also contribute to the failure of anti-EGFR treatment[10,11]. Similarly, a urokinase receptor–Bim signaling axis may also contribute to EGFR inhibition resistance[13].

GBM is a devastating and intractable disease. Temozolomide is the first-line chemotherapy drug used in GBM and, in combination with surgery and radiation, results in a modest increase in overall survival of patients[50]. No targeted treatment has proven effective in GBM. Our data indicate that EGFR inhibition may be effective if combined with inhibition of a component of the TNF–JNK–Axl–ERK signaling axis. Remarkably, the combined inhibition of EGFR and the TNF pathway was effective even in established GBM cell lines that are otherwise completely resistant to EGFR inhibition. The identification of this TNF–JNK–Axl–ERK signaling axis suggests that it may be possible to target and inhibit this adaptive response at multiple nodes, alone or in combination. We have found EGFR inhibition in conjunction with JNK inhibition to be effective in an animal model. Additionally, a combination of EGFR inhibition and thalidomide was also very effective in suppressing the growth of GBM tumors in both a subcutaneous and an intracranial animal model. Thalidomide crosses the blood-brain barrier and, indeed, has been previously used clinically in GBM without success[35]. This is consistent with our results that show no effect of thalidomide in the absence of EGFR inhibition. Notably, this approach was effective in both EGFRwt and mutant EGFRvIII-expressing tumors. EGFR expression is detected in most GBMs, and thus this approach could be broadly applicable in this disease. Furthermore, a rapid translation of these findings to the clinic is possible, given the wealth of TNF-inhibiting drugs and biologicals in clinical practice, including drugs such as thalidomide that penetrate the blood-brain barrier.

METHODS

Methods, including statements of data availability and any associated accession codes and references, are available in the online version of the paper.

1. Sharma, S.V., Bell, D.W., Settleman, J. & Haber, D.A. Epidermal growth factor receptor mutations in lung cancer. *Nat. Rev. Cancer* **7**, 169–181 (2007).
2. Arteaga, C.L. & Engelman, J.A. ERBB receptors: from oncogene discovery to basic science to mechanism-based cancer therapeutics. *Cancer Cell* **25**, 282–303 (2014).
3. Chong, C.R. & Jänne, P.A. The quest to overcome resistance to EGFR-targeted therapies in cancer. *Nat. Med.* **19**, 1389–1400 (2013).
4. Fan, W. *et al.* MET-independent lung cancer cells evading EGFR kinase inhibitors are therapeutically susceptible to BH3 mimetic agents. *Cancer Res.* **71**, 4494–4505 (2011).
5. Lee, H.J. *et al.* Drug resistance via feedback activation of Stat3 in oncogene-addicted cancer cells. *Cancer Cell* **26**, 207–221 (2014).
6. Verhaak, R.G. *et al.* Integrated genomic analysis identifies clinically relevant subtypes of glioblastoma characterized by abnormalities in PDGFRA, IDH1, EGFR, and NF1. *Cancer Cell* **17**, 98–110 (2010).
7. Hatanpaa, K.J., Burma, S., Zhao, D. & Habib, A.A. Epidermal growth factor receptor in glioma: signal transduction, neuropathology, imaging, and radioresistance. *Neoplasia* **12**, 675–684 (2010).
8. Mellinghoff, I.K. *et al.* Molecular determinants of the response of glioblastomas to EGFR kinase inhibitors. *N. Engl. J. Med.* **353**, 2012–2024 (2005).
9. Karpel-Massler, G., Schmidt, U., Unterberg, A. & Halatsch, M.E. Therapeutic inhibition of the epidermal growth factor receptor in high-grade gliomas: where do we stand? *Mol. Cancer Res.* **7**, 1000–1012 (2009).
10. Akhavan, D. *et al.* De-repression of PDGFRβ transcription promotes acquired resistance to EGFR tyrosine kinase inhibitors in glioblastoma patients. *Cancer Discov.* **3**, 534–547 (2013).
11. Nathanson, D.A. *et al.* Targeted therapy resistance mediated by dynamic regulation of extrachromosomal mutant EGFR DNA. *Science* **343**, 72–76 (2014).
12. Barkovich, K.J. *et al.* Kinetics of inhibitor cycling underlie therapeutic disparities between EGFR-driven lung and brain cancers. *Cancer Discov.* **2**, 450–457 (2012).
13. Wykosky, J. *et al.* A urokinase receptor-Bim signaling axis emerges during EGFR inhibitor resistance in mutant EGFR glioblastoma. *Cancer Res.* **75**, 394–404 (2015).
14. Chakraborty, S. *et al.* Constitutive and ligand-induced EGFR signalling triggers distinct and mutually exclusive downstream signalling networks. *Nat. Commun.* **5**, 5811 (2014).
15. Guo, G. *et al.* Ligand-independent EGFR signaling. *Cancer Res.* **75**, 3436–3441 (2015).
16. Acquaviva, J. *et al.* Chronic activation of wild-type epidermal growth factor receptor and loss of Cdkn2a cause mouse glioblastoma formation. *Cancer Res.* **71**, 7198–7206 (2011).
17. Endres, N.F. *et al.* Conformational coupling across the plasma membrane in activation of the EGF receptor. *Cell* **152**, 543–556 (2013).
18. Ramnarain, D.B. *et al.* Differential gene expression analysis reveals generation of an autocrine loop by a mutant epidermal growth factor receptor in glioma cells. *Cancer Res.* **66**, 867–874 (2006).
19. Wong, A.J. *et al.* Structural alterations of the epidermal growth factor receptor gene in human gliomas. *Proc. Natl. Acad. Sci. USA* **89**, 2965–2969 (1992).
20. Gil Del Alcazar, C.R., Todorova, P.K., Habib, A.A., Mukherjee, B. & Burma, S. Augmented HR repair mediates acquired temozolomide resistance in glioblastoma. *Mol. Cancer Res.* **14**, 928–940 (2016).
21. Pingle, S.C. *et al.* *In silico* modeling predicts drug sensitivity of patient-derived cancer cells. *J. Transl. Med.* **12**, 128 (2014).

22. Puliyappadamba, V.T. *et al.* Opposing effect of EGFRWT on EGFRvIII-mediated NF-κB activation with RIP1 as a cell death switch. *Cell Rep.* **4**, 764–775 (2013).
23. Sarkaria, J.N. *et al.* Use of an orthotopic xenograft model for assessing the effect of epidermal growth factor receptor amplification on glioblastoma radiation response. *Clin. Cancer Res.* **12**, 2264–2271 (2006).
24. Stommel, J.M. *et al.* Coactivation of receptor tyrosine kinases affects the response of tumor cells to targeted therapies. *Science* **318**, 287–290 (2007).
25. Huang, P.H. *et al.* Quantitative analysis of EGFRvIII cellular signaling networks reveals a combinatorial therapeutic strategy for glioblastoma. *Proc. Natl. Acad. Sci. USA* **104**, 12867–12872 (2007).
26. Pillay, V. *et al.* The plasticity of oncogene addiction: implications for targeted therapies directed to receptor tyrosine kinases. *Neoplasia* **11**, 448–458 (2009).
27. Greenall, S.A. *et al.* EGFRvIII-mediated transactivation of receptor tyrosine kinases in glioma: mechanism and therapeutic implications. *Oncogene* **34**, 5277–5287 (2015).
28. Awad, A.J., Burns, T.C., Zhang, Y. & Abounader, R. Targeting MET for glioma therapy. *Neurosurg. Focus* **37**, E10 (2014).
29. Zhu, Y. & Shah, K. Multiple lesions in receptor tyrosine kinase pathway determine glioblastoma response to pan-ERBB inhibitor PF-00299804 and PI3K/mTOR dual inhibitor PF-05212384. *Cancer Biol. Ther.* **15**, 815–822 (2014).
30. Blakely, C.M. *et al.* NF-κB-activating complex engaged in response to EGFR oncogene inhibition drives tumor cell survival and residual disease in lung cancer. *Cell Rep.* **11**, 98–110 (2015).
31. Wajant, H., Pfizenmaier, K. & Scheurich, P. Tumor necrosis factor signaling. *Cell Death Differ.* **10**, 45–65 (2003).
32. Higuchi, M. & Aggarwal, B.B. TNF induces internalization of the p60 receptor and shedding of the p80 receptor. *J. Immunol.* **152**, 3550–3558 (1994).
33. Deng, L., Ding, W. & Granstein, R.D. Thalidomide inhibits tumor necrosis factor-alpha production and antigen presentation by Langerhans cells. *J. Invest. Dermatol.* **121**, 1060–1065 (2003).
34. Gross, N.D. *et al.* Inhibition of Jun NH2-terminal kinases suppresses the growth of experimental head and neck squamous cell carcinoma. *Clin. Cancer Res.* **13**, 5910–5917 (2007).
35. Groves, M.D. *et al.* A North American Brain Tumor Consortium (NABTC 99-04) phase II trial of temozolomide plus thalidomide for recurrent glioblastoma multiforme. *J. Neurooncol.* **81**, 271–277 (2007).
36. Gu, X. *et al.* Intraperitoneal injection of thalidomide attenuates bone cancer pain and decreases spinal tumor necrosis factor-α expression in a mouse model. *Mol. Pain* **6**, 64 (2010).
37. Prahallad, A. *et al.* Unresponsiveness of colon cancer to BRAF(V600E) inhibition through feedback activation of EGFR. *Nature* **483**, 100–103 (2012).
38. Duncan, J.S. *et al.* Dynamic reprogramming of the kinome in response to targeted MEK inhibition in triple-negative breast cancer. *Cell* **149**, 307–321 (2012).
39. Huang, P.H., Xu, A.M. & White, F.M. Oncogenic EGFR signaling networks in glioma. *Sci. Signal* **2**, re6 (2009).
40. Li, L. *et al.* An EGFR wild type-EGFRvIII-HB-EGF feed-forward loop regulates the activation of EGFRvIII. *Oncogene* **33**, 4253–4264 (2014).
41. Fan, Q.W. *et al.* EGFR phosphorylates tumor-derived EGFRvIII driving STAT3/5 and progression in glioblastoma. *Cancer Cell* **24**, 438–449 (2013).
42. Jahani-Asl, A. *et al.* Control of glioblastoma tumorigenesis by feed-forward cytokine signaling. *Nat. Neurosci.* **19**, 798–806 (2016).
43. de la Iglesia, N. *et al.* Identification of a PTEN-regulated STAT3 brain tumor suppressor pathway. *Genes Dev.* **22**, 449–462 (2008).
44. Rich, J.N. *et al.* Phase II trial of gefitinib in recurrent glioblastoma. *J. Clin. Oncol.* **22**, 133–142 (2004).
45. Brown, P.D. *et al.* Phase I/II trial of erlotinib and temozolomide with radiation therapy in the treatment of newly diagnosed glioblastoma multiforme: North Central Cancer Treatment Group Study N0177. *J. Clin. Oncol.* **26**, 5603–5609 (2008).
46. Peereboom, D.M. *et al.* Phase II trial of erlotinib with temozolomide and radiation in patients with newly diagnosed glioblastoma multiforme. *J. Neurooncol.* **98**, 93–99 (2010).
47. Schuster, J. *et al.* A phase II, multicenter trial of rindopepimut (CDX-110) in newly diagnosed glioblastoma: the ACT III study. *Neuro-oncol.* **17**, 854–861 (2015).
48. Inda, M.D. *et al.* Tumor heterogeneity is an active process maintained by a mutant EGFR-induced cytokine circuit in glioblastoma. *Genes Dev.* **24**, 1731–1745 (2010).
49. Furnari, F.B., Cloughesy, T.F., Cavenee, W.K. & Mischel, P.S. Heterogeneity of epidermal growth factor receptor signalling networks in glioblastoma. *Nat. Rev. Cancer* **15**, 302–310 (2015).
50. Stupp, R. *et al.* Radiotherapy plus concomitant and adjuvant temozolomide for glioblastoma. *N. Engl. J. Med.* **352**, 987–996 (2005).

ONLINE METHODS

Plasmids, transfection and generation of cell lines. Primary GBM neurosphere cultures were generated directly from human GBM tumor specimens. Cells were cultured in DMEM F12 supplemented with B27 without vitamin A and with EGF (20 ng/ml) and bFGF (20 ng/ml). GBM9 was provided by James Van Brocklyn and GBM39 was provided by C. David James via Frank Furnari. U87EGFRwt and U87EGFRvIII cells were provided by Frank Furnari and have been described previously[48]. U251MG cells expressing EGFRwt were generated as we have described previously[14]. Cell lines were authenticated using a Promega StemElite ID system, which is an STR based assay. Cell lines were tested for mycoplasma contamination using a MycoAlert kit from Lonza (Basel, Switzerland, catalog #LT 07-218). NF-κB-LUC plasmid was provided by Ezra Burstein (UT Southwestern). The 3xAP1pGL3 reporter plasmid was obtained from Addgene (40342).

Luciferase assays. Cells were plated in 48-well dishes to 70–80% confluence, followed by transfection with NF-κB-LUC or 3xAP1pGL3 reporter plasmid using Lipofectamine 2000. A dual-luciferase reporter assay system was used according to manufacturer's instructions (Promega, Madison, WI). Firefly luciferase activity was measured in a luminometer and normalized on the basis of *Renilla* luciferase activity. Experiments were done in triplicate and three independent experiments were performed.

RNA interference. For transient silencing we used a pool of siRNA sequences directed against human TNFR1, Axl, JNK1, JNK2 or control (scrambled), obtained from Santa Cruz. siRNAs were introduced into cells using the Lipofectamine 2000 (Invitrogen, Carlsbad, CA) according to the manufacturer's instructions. Experiments were conducted 48 h after siRNA transfection. Knockdown efficiency was confirmed by western blotting.

Antibodies, reagents and western blotting. Western blot analysis was performed according to standard protocols. In all experiments, before the addition of EGF or erlotinib, established cells were cultured overnight in serum-free DMEM and primary GBM neurospheres were EGF starved overnight. Cells not treated with EGF or erlotinib were also serum or EGF starved. EGFR antibody (06-847, 1 µg/ml) was from Millipore. pEGFR-1068 (2236), pERK (4376) ERK (4695), p34 (9251), JNK (9252), STAT3 (9139), pAkt (0915) and pSTAT3 (9131) antibodies were from Cell Signaling Technology (Danvers, MA) and were used at 1:1,000 dilution; TNFR1 (sc-8436), ERK2 (sc-154), Akt (sc-1619) and β-actin (sc-47778) antibodies were from Santa Cruz Biotechnology (Dallas, TX) were used at a concentration of 1 µg/ml. GAS6 (AF885), pAxl (AF2228) and Axl (AF154) antibodies were from R&D Biosystems (Minneapolis, MN) and were used at a concentration of 1 µg/ml. c-JUN antibody (ab31419) was from Abcam (Cambridge, MA) and was used at 2 µg per ChIP reaction. Human TNF-α antibody (MAB610) was from R&D Biosystems and was used at 2 µg/ml. Full-length western blots are shown in **Supplementary Figures 11–15**.

Reagents. Recombinant human TNF and EGF were obtained from Peprotech (Rocky Hill, NJ). Erlotinib and XL765 were purchased from SelleckChem (Houston, TX). Afatinib was bought from AstaTech, Inc. (Bristol, PA). The Axl inhibitor R428, the ERK inhibitor U0126 and thalidomide were from Cayman Chemical (Ann Arbor, MI). Etanercept (Enbrel) was purchased from McKesson Medical Supply (San Francisco, CA). The JNK inhibitor SP600125, p38 inhibitor SB203580 and NF-κB inhibitor BMS-345541 were obtained from EMD Millipore (Billerica, MA). Necrostatin-1 was obtained from Fisher Scientific (Pittsburgh, PA). Lipopolysaccharide was purchased from Sigma (St. Louis, MO). Cetuximab was provided by ImClone and used at a concentration of 10 µg/ml overnight.

Chromatin immunoprecipitation assay. GBM9 and U87EGFRwt cells were cultured in one 15-cm plate per reaction. ChIP assays were carried out using a ChIP chromatin immunoprecipitation kit (Millipore) following the manufacturer's instructions. The ChIP-enriched DNA samples were quantified by PCR using Platinum Taq DNA polymerase (Invitrogen). Putative AP-1 binding sites on the *GAS6* promoter were predicted using the TFBIND program (http://tfbind.hgc.jp/). The following primer pairs covering AP-1 sites were used: 5′-GGA TCTGACCTCAGTGTATC-3′ and 5′-TGGTTGTCTTCACTAGCGAT-3′.

cDNA synthesis and real-time PCR. Total RNA was isolated by TRIzol reagent (Ambion). cDNA reverse transcriptions were performed by using the High-Capacity cDNA Reverse Transcription Kit (Applied Biosystems). PCR primers were synthesized by IDT (Coralville, IA). Each PCR was carried out in triplicate in a 20-µl volume using SYBR Green Master Mix (Applied Biosystems) for 15 min at 95 °C for initial denaturing, followed by 40 cycles of 95 °C for 15 s and 60 °C for 60 s in a ViiA 7 Real-Time PCR System (Applied Biosystems). At least two independent experiments were done. Values for each gene were normalized to expression levels of *GAPDH* mRNA. The following primers were used. *TNF*, 5′-CCCAGGGACCTCTCTCTAATCA-3′ and 5′-GCTACAGGCTTGTCACTC GG-3′; *GAS6*, 5′-CATCAACAAGTATGGGTCTCCGT-3′ and 5′-GTTCTCCT GGCTGCATTCGTTGA-3′; *GAPDH*, 5′-GTGAAGGTCGGAGTCAACGG-3′ and 5′-TGATGACAAGCTTCCCGTTCTC-3′.

ELISA. 2×10^6 cells were incubated in serum-free or EGF-free medium containing different concentrations of erlotinib or DMSO. After 48 h, supernatant and cell lysates were collected. Supernatant medium was concentrated 5- to 10-fold with a Pierce protein concentrator (ThermoFisher). TNF protein concentration in supernatant, cell lysates and tissue extracts was determined by ELISA using a commercial TNF detection kit (ThermoFisher) according to the manufacturer's instructions. Additionally, GAS6 protein concentration in supernatant was measured by ELISA kit (LifeSpan BioSciences).

Cell viability assay. The cell viability assay was conducted using an AlamarBlue cell viability assay kit (ThermoFisher) following the manufacturer's protocol. Cells were cultured in Corning 96-well black plates with clear bottoms (5,000 cells per well). Drugs were added to cells for 72 h, followed by detection using a POLARstar Omega microplate reader (excitation at 544 nm and emission at 590 nm) (BMG Labtech, Germany).

Animal studies. Female athymic nude mice 4–6 weeks old were purchased from Charles River Laboratories. The mice were housed in plastic cages (4 or 5 mice per cage) in a room with a 12-h day-night cycle. GBM9 cells (1×10^6) were subcutaneously injected into the right flank of each nude mouse. By about 10 d after injection, all mice had developed subcutaneous tumors. The mice were randomly divided into control and treatment groups. Mice were treated with drugs using the indicated doses. For combination treatment, both drugs were given concurrently for the indicated periods. Tumor dimensions were measured by caliper every 2 d and tumor volumes calculated by the formula volume = length × width × width/2. Mice were sacrificed when tumors reached over 2,000 mm³ or at 24 d from the first day of treatment.

For the orthotopic model, 1×10^5 GBM9 cells expressing firefly luciferase were injected into the right corpus striatum of the brains of 6- to 8-week-old nude mice using a stereotactic frame. When tumors became apparent by bioluminescence imaging (7 d after injection), mice were randomly divided into four groups (control gavage group, afatinib group, thalidomide group and afatinib + thalidomide group, $n = 8$ per group). The mice were treated with erlotinib 50 mg/kg by oral gavage and/or intraperitoneal injection of 150 mg/kg thalidomide for 10 consecutive days. Bioluminescence imaging was performed to record the growth of tumors every 5 d. Kaplan–Meier survival curves were calculated using GraphPad Prism 7.0 software. Mice were monitored and sacrificed when neurological signs appeared or after 40 d.

To quantify *in vivo* TNF, 1×10^6 GBM9 cells were injected into the right flanks of nude mice. When the subcutaneous tumor reached a volume of around 200 mm³, the mice were treated with erlotinib to monitor the upregulation of TNF protein. The animals were dosed consecutively for 1, 2, 7 or 14 d and then sacrificed. Animals without treatment were considered controls (0 day treatment). Tumor tissues were rinsed in PBS and protein was extracted to analyze TNF levels using ELISA and also used for western blot. To detect protein expression in mice brain tumor tissues upon drug treatment, the same procedure was performed in orthotopic models. Additionally, in orthotopic models, mice were divided into four groups (control group, erlotinib group, thalidomide group and erlotinib plus thalidomide, $n = 3$). After 48 h treatment, tumors were collected and subjected to western blot and immunostaining.

All animal studies were done under Institutional Animal Care and Use Committee-approved protocols at the University of Texas Southwestern Medical Center and the VA North Texas Health Care System.

Immunohistochemistry. Tumors from nude mice brains were fixed in 10% formalin and embedded in paraffin. Paraffin-embedded sections were cut at 5 μm thickness. Immunohistochemical staining was performed using the ABC streptavidin–biotin method with the Vectastain ABC kit (Vector Laboratories, Burlingame, CA, USA) according to the manufacturer's protocol. Briefly, after deparaffinization and rehydration, endogenous peroxidase activity was quenched by a 10-min incubation in 3% H_2O_2. For antigen retrieval, the tissue sections were boiled in 10 mM sodium citrate buffer (pH 6.0) for 20 min. Binding of primary anti-pERK (1:100, Cell Signaling Technology, 4376), anti-pJNK antibody (1:200, Cell Signaling Technology, 4668) or anti-pAxl (1:400, R&D, AF2228) was carried out overnight at 4 °C. The signal was detected using Sigmafast 3,3′-diaminobenzi-dine tablets (DAB; Sigma, St. Louis MO). The sections were counterstained lightly with hematoxylin. The immunohistochemistry staining intensity was scored semiquantitatively as follows: 0 = no positive staining; 1 = 1–25% of tumor cells stained, 2 = 26–75% of tumor cells stained and 3 = >75% of tumor cells stained.

Cell death annexin assay. The annexin assay was performed by using an Annexin-V-FLUOS staining kit (Roche applied Science). Cells (1×10^6) were plated in six-well plates and treated with drugs or vehicle alone. After 72 h cells were trypsinized and washed twice with PBS. The cells were incubated for 15 min at room temperature with propidium iodide and Annexin-V-FLUOS labeling solution in incubation buffer. Annexin- and/or propidium iodide–positive cells were detected by flow cytometry.

Caspase-3/7 activity. Caspase activity in the supernatant was measured using the Caspase-Glo 3/7 Assay (Promega, G8091) following manufacturer's instructions. Briefly, 72 h after treatment cells were washed by cold PBS and total cell lysates were prepared. 50 μg of total protein per sample were added per well of a 96-well plate and the samples incubated with 100 μl caspase 3/7 reagent for 30 min. The luminescence of each sample was measured using a luminometer. All experiments included at least 3 replicates per group and were repeated 3 times.

Statistical analysis. All data were analyzed for significance using GraphPad Prism 7.0 software. Error bars represent the means ± s.e.m. of three independent experiments if not indicated. We used 8 mice per group based on power analysis. This sample size calculation is based upon tumor volume measured at 4 weeks after drug administration. Specifications and assumptions for this calculation are (i) a tumor volume change of 50% for the treated group as compared with the control group, (ii) a s.d. of 30% for tumor volume in each of the comparison groups, (iii) power of 85% and two-sided type I error rate of 5%, and (iv) use of two-sample t-test (total mice: 32). Two-tailed unpaired Student's t-tests were used for comparison of two data sets. The Mann-Whitney U test was applied to test the significant differences in immunohistochemistry staining intensity between different groups. Data distribution was assumed to be normal, but this was not formally tested. Samples and animals were randomized for experimentation; data collection and analysis were not performed blind to the conditions of the experiments. At least 3 independent molecular and biochemical analyses were performed unless otherwise indicated. $P < 0.05$ was considered statistically significant. In figures, $*P < 0.05$, $**P < 0.01$, $***P < 0.001$ and $****P < 0.0001$.

A **Supplementary Methods Checklist** is available.

Data availability. The data supporting the findings of this study are available from the corresponding author upon reasonable request.